Electronic Supplementary Information

Insight into the decay mechanism of cycling capacitance for layered double hydroxides at subnanometer scale

Jie Zhao, Yue Guo, Yuqi Yang, Zhen Shen, Qiang Wu*, Lijun Yang, Xizhang Wang, Zheng Hu*

Key Laboratory of Mesoscopic Chemistry of MOE, School of Chemistry and Chemical Engineering, Nanjing University, Nanjing 210023, China.

*Corresponding authors.

E-mail address: wqchem@nju.edu.cn; zhenghu@nju.edu.cn.

Experimental

Preparation of NiCo-LDH samples. The NiCo-LDH samples were prepared by the coprecipitation reaction, as we reported previously.[S1-S3] Typically, $Ni(NO_3)_2 \cdot 6H_2O$ (15 mmol, 4.362 g) and $Co(NO_3)_2 \cdot 3H_2O$ (5 mmol, 1.208 g) were dissolved into 100 mL distilled water, and then 10 mL of a degassed aqueous solution containing hexamethylenetetramine (HMT, 20 mmol, 2.804 g) and $H_2C_2O_4 \cdot 2H_2O$ (0.10 g) was added by a syringe under stirring. This mixture was refluxed at 100 ℃ for 6 h under an oxygen atmosphere to avoid CO_2 interference. The product was obtained by filtrating, repeated washing, and drying in a vacuum oven at 80 ℃, which has the charge-balancing NO_3^- anions, denoted as NiCo-LDH/NO_3^-. For increasing the interlayer distance, the replacement of NO_3^- with larger anions (*i.e.*, 1,4-benzenedicarboxylic anions) were performed.[S1] Typically, NiCo-LDH/NO_3^- (100 mg) was added into 100 mL degassed solution containing 1,4-benzenedicarboxylic sodium ($C_6H_4(COO)_2Na_2$) (10 mmol, 2.101 g) and refluxed at 90 ℃ for 24 h under oxygen atmosphere. Then, the final sample was obtained by washing and drying, denoted as NiCo-LDH/CBD.

Encapsulation of NiCo-LDH/CBD with sodium polyacrylate (PA). The NiCo-LDH/NO_3^- (100 mg), 1,4-benzenedicarboxylic sodium ($C_6H_4(COO)_2Na_2$) (10 mmol, 2.101 g), and sodium acrylate (5 mmol, 0.47 g) were put into 100 mL degassed distilled water and refluxed at 90 °C for 24 h under oxygen atmosphere. Then, 50 mg of the obtained powder sample was added into 15 mL isopropanol containing 1 mL aqueous solution of ammonium peroxydisulfate (0.028 g mL^{-1}) and stirred for 1 h at room temperature. The product was obtained by ethanol washing and drying in a vacuum oven at 80 ℃ for 12 h, denoted as NiCo-LDH/CBD-PA.

Materials characterization. The morphology of the samples was characterized by scanning electron microscope (SEM, Hitachi S-4800) and transmission electron microscope (TEM, FEI Tecnai F20). The interlayer distance of obtained samples was measured by X-ray diffraction (XRD, Bruker D8 Advance A25 Co Kα radiation of 1.7902 Å). Fourier transform infrared spectroscopy (FT-IR, Bruker VERTEX70) was used to examine the anion species in LDHs during the cycling.

Electrochemical measurements. The electrochemical performances were evaluated on a VMP3 workstation (Biologic) using a three-electrode cell in 6 M KOH aqueous solution (with or without 0.5 M K_2CO_3), with platinum foil counter electrode and Ag/AgCl reference electrode. The working electrode was prepared by coating the slurry of LDH, acetylene black, and polyvinylidene fluoride (with a weight ratio of 8:1.5:0.5) on Ni foam. The specific capacitances and cycling stability were tested by the galvanostatic charge/discharge (GCD) method. The cyclic voltammetry (CV) curves were tested at a scan rate of 20 mV s^{-1} during the long-term charge/discharge tests. The electrochemical impedance spectra (EIS) were tested at a frequency range of 100KHz~10mHz with an applied potential of 0.25 V (*vs.* Ag/AgCl). The weight retentions of samples were measured on a thermal gravimetric analyzer (Pyris 1, Perkin Elmer) under N_2 with a heating rate of 5 °C min^{-1}. The specific capacitances (C_W, F g^{-1}) were calculated by the following equation: $C_W = (I \times \Delta t) / (m \times \Delta V)$, where I is the discharge current (A), Δt is the discharge time (s), ΔV is the voltage range (V), and m is the mass of LDHs samples (g). The capacitance contributed by the bare Ni foam was subtracted.

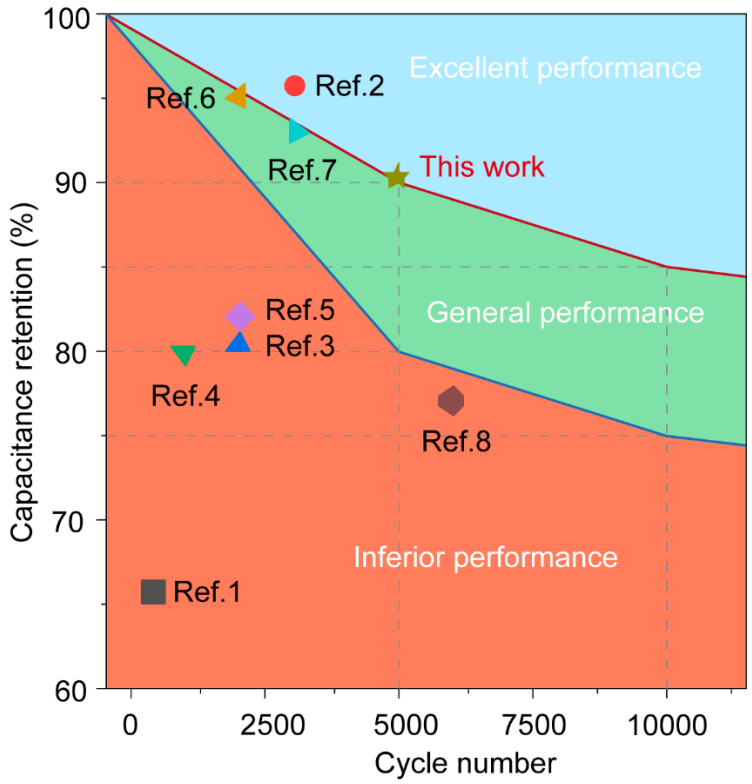

Fig. S1. The cycling performance of various LDHs electrodes.

The data from the literatures are listed below.

Ref. 1_$Co^{II}Co^{III}$-LDH (cycling at 2 A g^{-1} for 300 cycles) [S4]

Ref. 2_NiCo-LDH/ZnO (cycling at 2 A g^{-1} for 3000 cycles) [S5]

Ref. 3_CoFe-LDH (cycling at 4 A g^{-1} for 2000 cycles) [S6]

Ref. 4_NiFe-LDH (cycling at 5 A g^{-1} for 1000 cycles) [S7]

Ref. 5_NiCoAl-LDH (cycling at 5 A g^{-1} for 2000 cycles) [S8]

Ref. 6_$Co^{II}Co^{III}$-LDH (cycling at 5 A g^{-1} for 2000 cycles) [S9]

Ref. 7_NiCoAl-LDH (cycling at 6 A g^{-1} for 3000 cycles) [S10]

Ref. 8_CoAl-LDH/Pt (cycling at 9 A g^{-1} for 6000 cycles) [S11]

Note: For better comparison, the literature data came from the pristine powder-like LDHs without any improvement. The capacitance retention was calculated according to $R = (C_{final}/C_{max}) \times 100\%$, where C_{final} is the capacitance of the final cycle, C_{max} is the maximum capacitance during cycling.

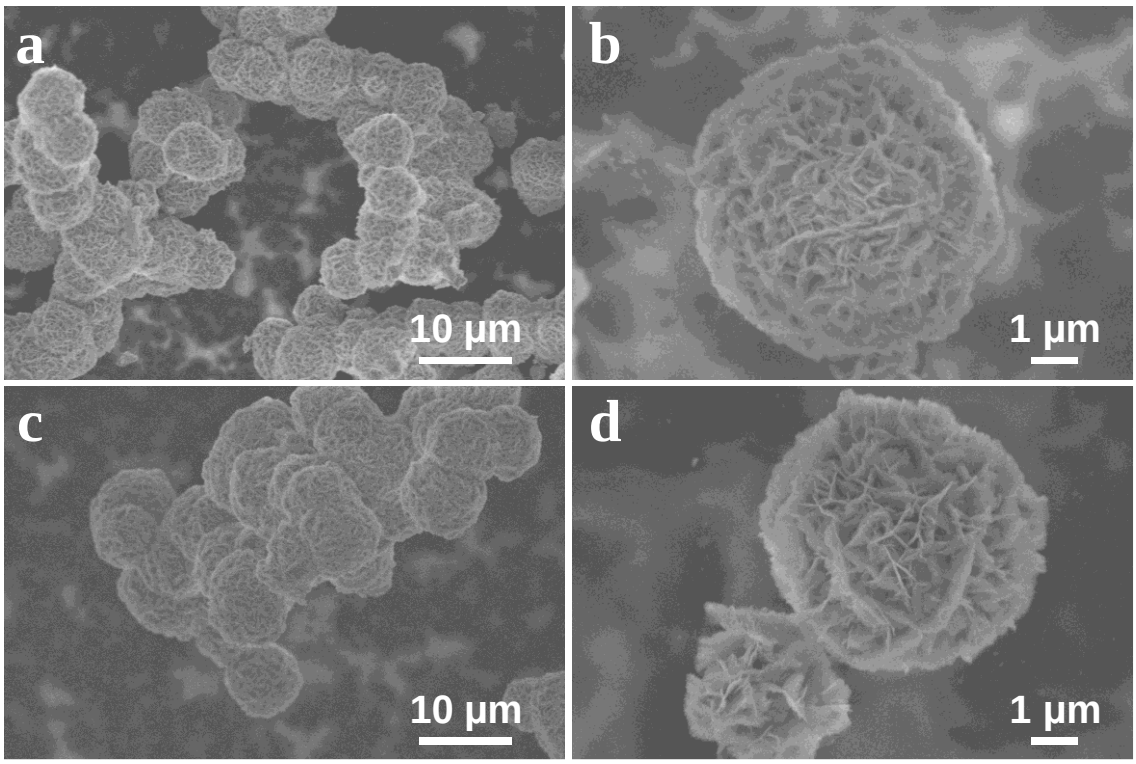

Fig. S2. SEM images of NiCo-LDH samples. (a, b) NiCo-LDH/CBD. (c, d) NiCo-LDH/NO_3^-.

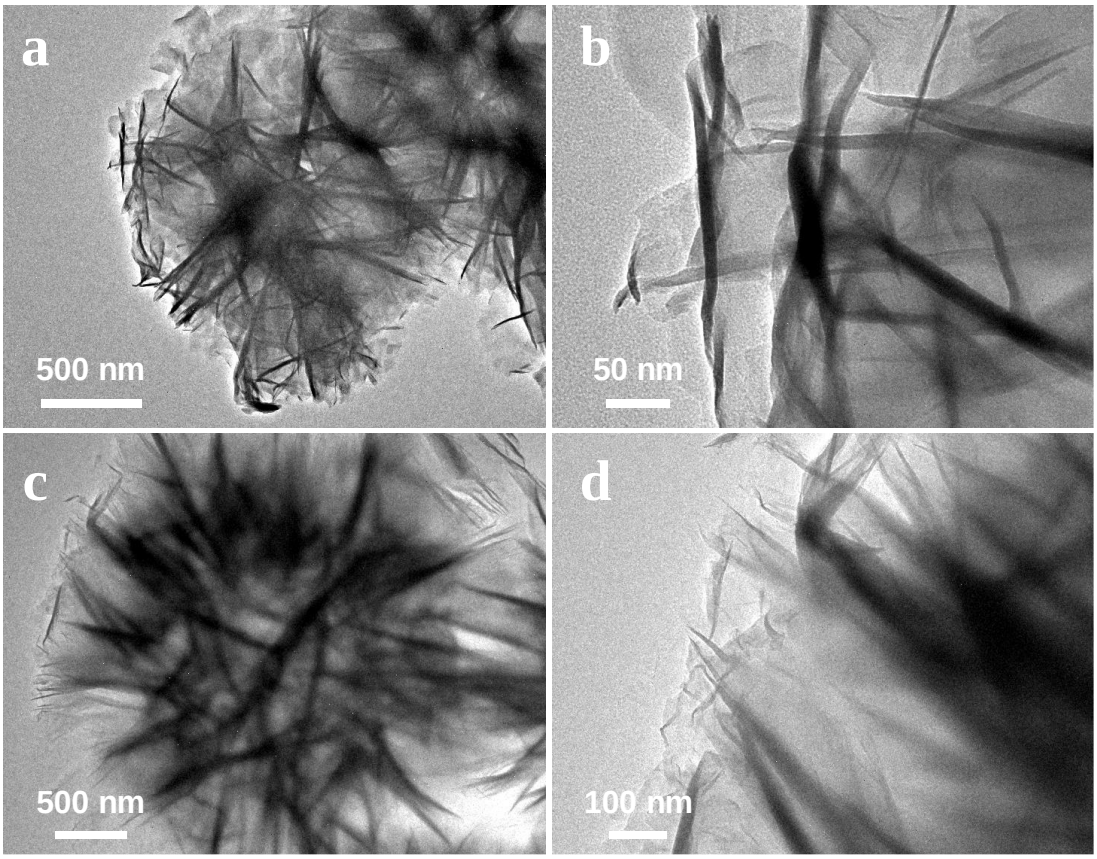

Fig. S3. TEM images of NiCo-LDHs samples. (a, b) NiCo-LDH/CBD. (c, d) NiCo-LDH/NO_3^-.

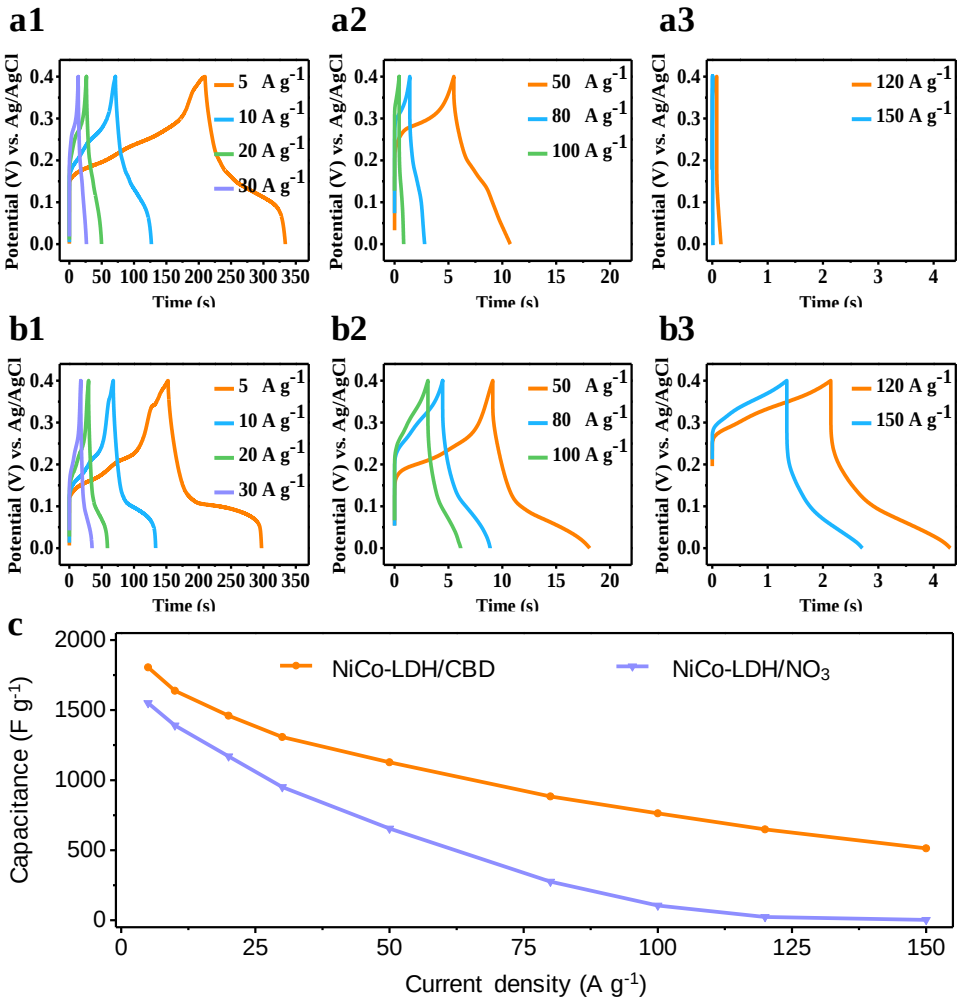

Fig. S4. GCD curves and rate performances of NiCo-LDH/NO_3^- and NiCo-LDH/CBD in 6 M KOH. (a1-a3) GCD curves of NiCo-LDH/NO_3^-. (b1-b3) GCD curves of NiCo-LDH/CBD. (c) The rate performances.

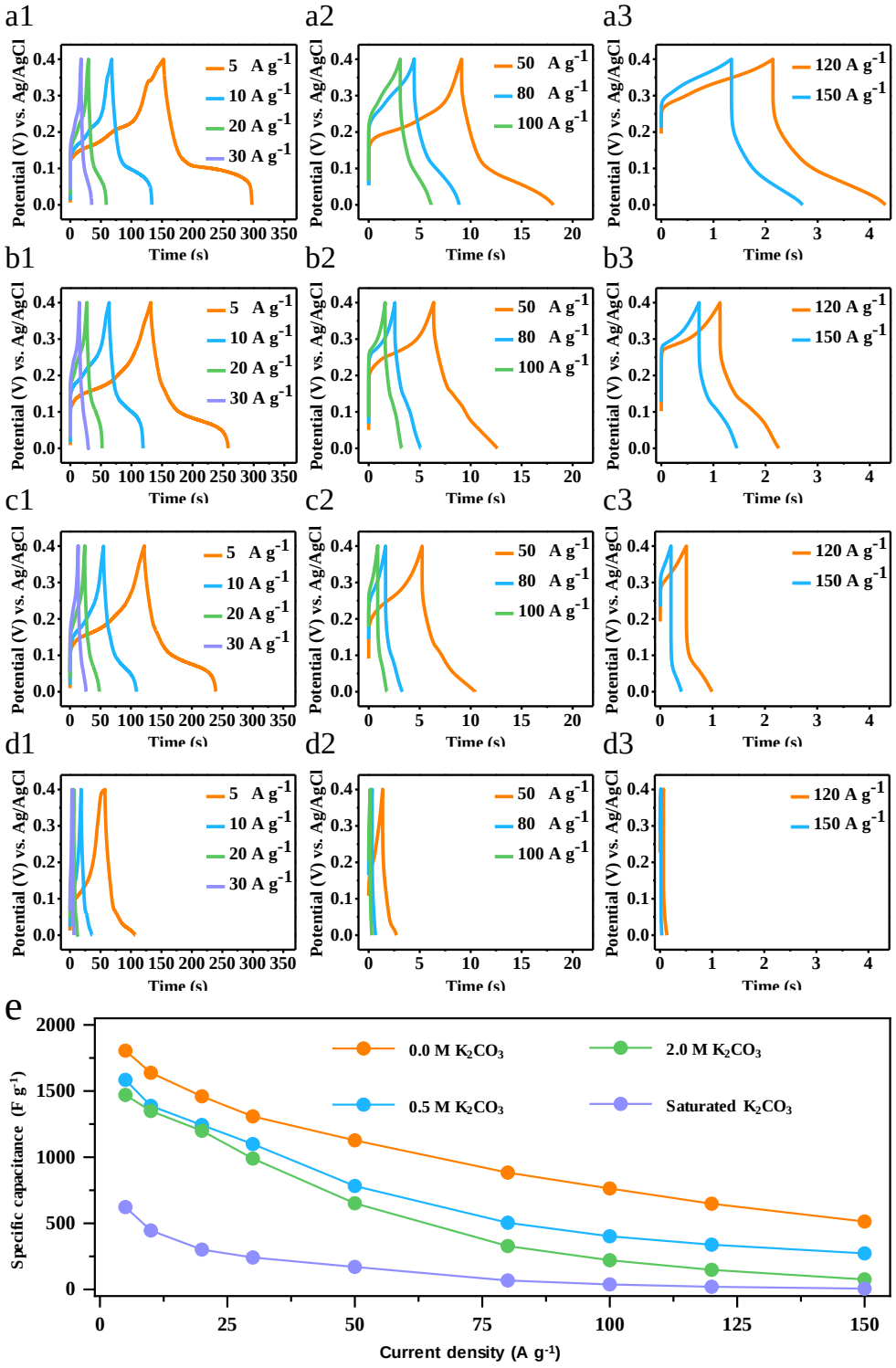

Fig. S5. GCD curves and rate performances of NiCo-LDH/CBD in 6 M KOH with different amounts of K_2CO_3. (a1-a3) GCD curves in 6 M KOH. (b1-b3) GCD curves in 6 M KOH with 0.5 M K_2CO_3. (c1-c3) GCD curves in 6 M KOH with 2.0 M K_2CO_3. (d1-d3) GCD curves in 6 M KOH with saturated K_2CO_3. (e) rate performances.

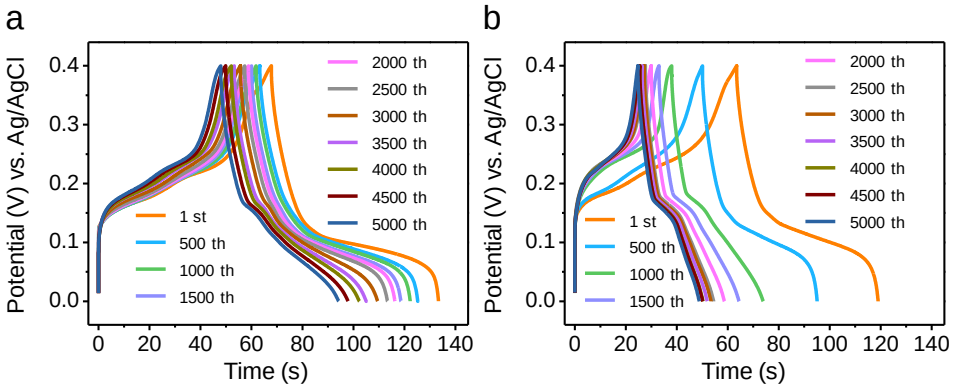

Fig. S6. GCD curves of NiCo-LDH/CBD at different cycles at 10 A g^{-1}. (a) in 6 M KOH. (b) in 6 M KOH with 0.5 M K_2CO_3.

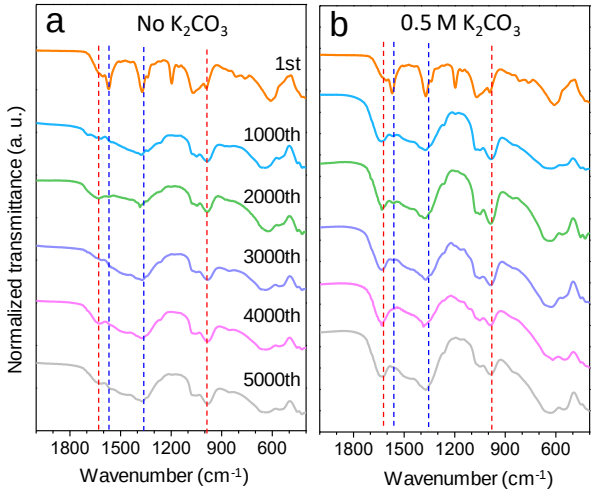

Fig. S7. The normalized FTIR transmittance spectra of NiCo-LDH/CBD during cycling in 6 M KOH with or without 0.5 M K_2CO_3 for different cycles. (a) In 6 M KOH without K_2CO_3. (b) In 6 M KOH with 0.5 M K_2CO_3.

After cycling in these two electrolytes, the intensities of the characteristic peaks at 993 cm^{-1} and 1636 cm^{-1} (corresponding to the C−O stretching vibration and the asymmetric C=O stretch for CO_3^{2-}, respectively, [S2] marked by the red dashed line) both increase. Meanwhile, the sharp peaks at 1370 cm^{-1} (corresponding to the symmetric COO^- stretch) and 1570 cm^{-1} (corresponding to the asymmetric COO^- stretch) for CBD anions both gradually weaken (marked by the blue dashed line).[S1] It is indicated that the CBD anions in the NiCo-LDH/CBD are exchanged by the CO_3^{2-} anions.

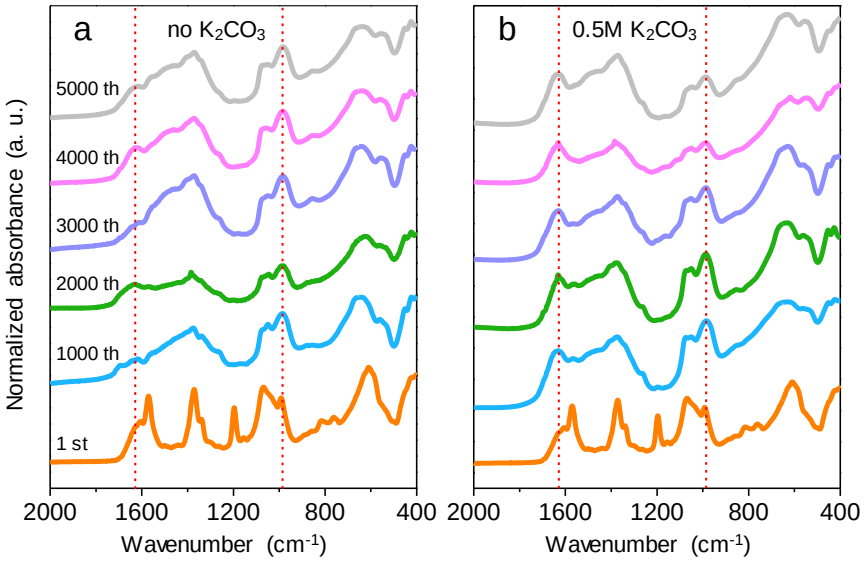

Fig. S8. The normalized FTIR absorbance spectra of NiCo-LDH/CBD after cycling in 6 M KOH with or without 0.5 M K_2CO_3 for different cycles. (a) In 6 M KOH without K_2CO_3. (b) In 6 M KOH with 0.5 M K_2CO_3.

The corresponding FTIR absorbance spectra were also measured. After cycling in these two electrolytes, the intensities of the characteristic peaks at 993 cm^{-1} and 1636 cm^{-1} (corresponding to the C−O stretching vibration and the asymmetric C=O stretch for CO_3^{2-}, respectively, [S2] marked by the red dashed line) both increase with increasing the cycle number, which reveals the intercalation of CO_3^{2-} anions into the interlayer space of NiCo-LDH to replace the CBD anions partly during cycling.

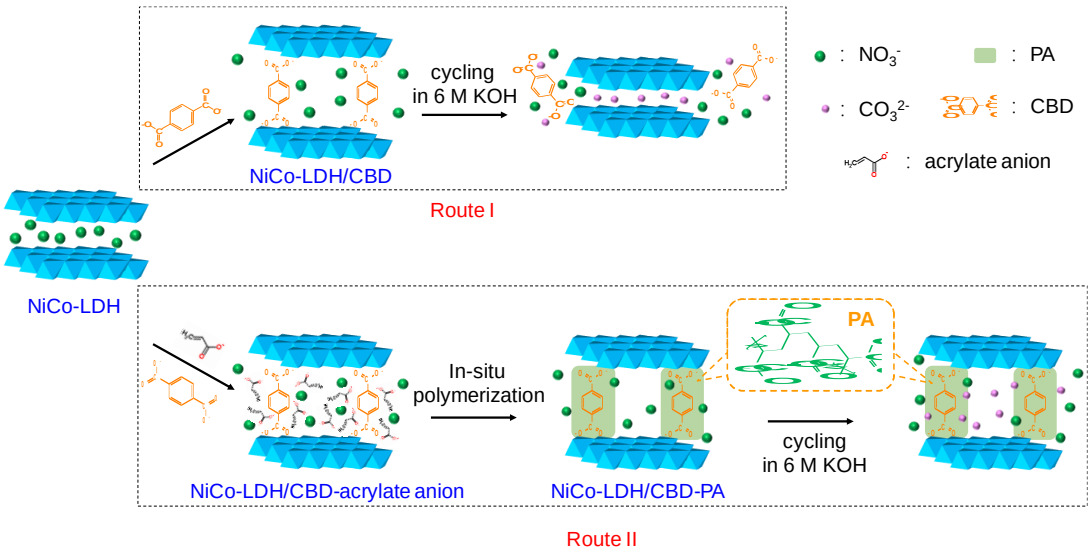

Fig. S9. Illustration of the PA encapsulation strategy for improving cycling stability of NiCo-LDH.

Route I: By using large-size CBD anions to replace the NO_3^- anions in NiCo-LDH/NO_3^-, the NiCo-LDH/CBD with a large interlayer distance was prepared. When cycling in the alkaline electrolyte with unavoidable CO_3^{2-} impurities, the CBD anions of NiCo-LDH/CBD would be replaced by CO_3^{2-} gradually, resulting in a narrow interlayer distance and the decreased capacitance.

Route II: By adding acrylate anions and CBD anions to replace the NO_3^- anions in NiCo-LDH/NO_3^-, the LDH sample with the intercalated CBD and acrylate anions was prepared. By in situ polymerizing the acrylate anions in the interlayers, the PA-encapsulated LDH, *i.e.*, NiCo-LDH/CBD-PA, was obtained. The PA polymer can partly inhibit the exchange of CBD by CO_3^{2-} during cycling, leading to a stable interlayer distance larger than the CO_3^{2-}-intercalated NiCo-LDH and thus a better cycling stability.

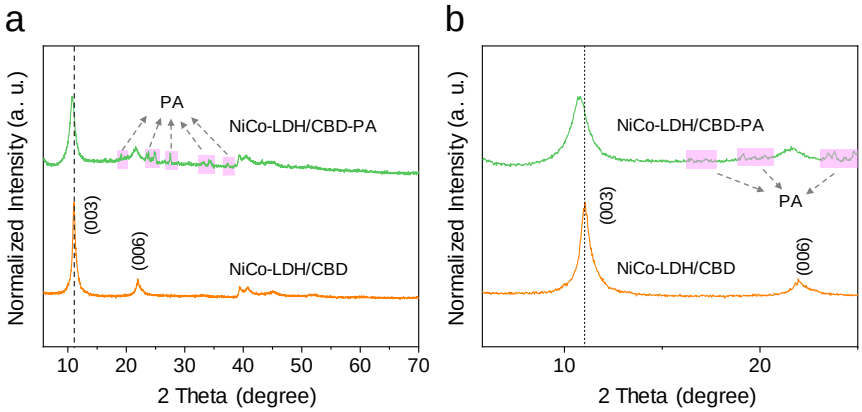

Fig. S10. The XRD patterns of NiCo-LDH/CBD and NiCo-LDH/CBD-PA in different 2-Theta ranges. (a) 5~70°. (b) 5~25°.

The XRD characteristic (003) peaks at 11.04° and 10.76° indicate the interlayer distances of 0.93 nm and 0.95 nm for NiCo-LDH/CBD and NiCo-LDH/CBD-PA, respectively. In addition, some new peaks were observed in the NiCo-LDH/CBD-PA, which is resulted from PA.

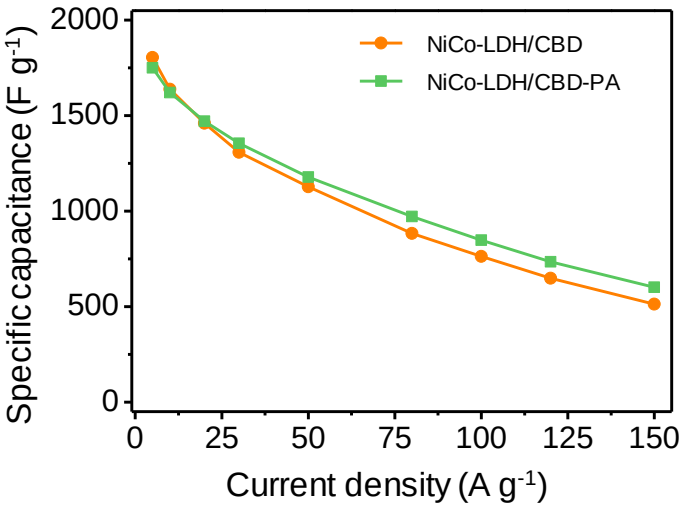

Fig. S11. The rate performances of the NiCo-LDH/CBD and NiCo-LDH/CBD-PA.

The specific capacitances were calculated based on the mass of NiCo-LDH/CBD. The mass ratio of NiCo-LDH/CBD in NiCo-LDH/CBD-PA was measured to be 88% by weighing the NiCo-LDH/CBD-PA sample before and after the alkaline solution treatment (see Fig. S15).

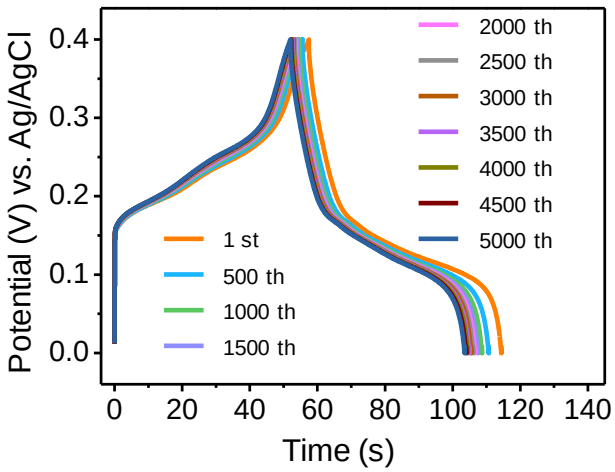

Fig. S12. The GCD curves of NiCo-LDH/CBD-PA at 10 A g^{-1} at different cycles in 6 M KOH solution.

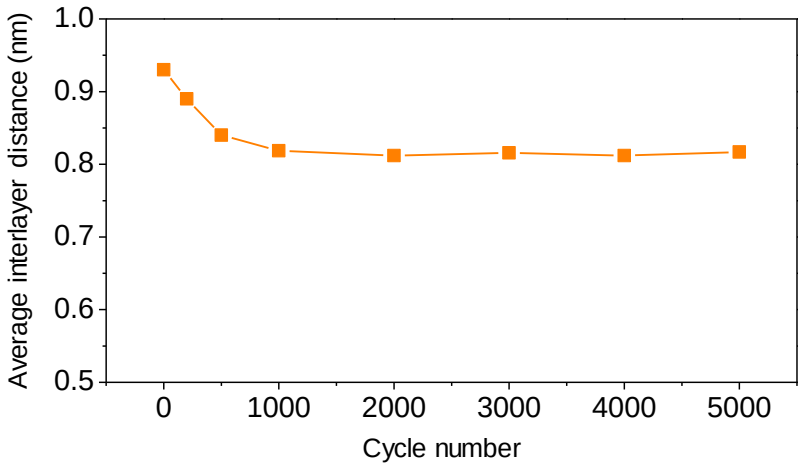

Fig. S13. The average interlayer distance of NiCo-LDH/CBD-PA after cycling in 6 M KOH for different cycles.

The interlayer distance of NiCo-LDH/CBD-PA decreases from 0.95 nm to 0.82 nm in the first 1000 cycles and then keeps constant (~0.82 nm) in the subsequent cycles. The interlayer distance of 0.82 nm is larger than that (0.76 nm) for NiCo-LDH/CBD without the PA encapsulation.

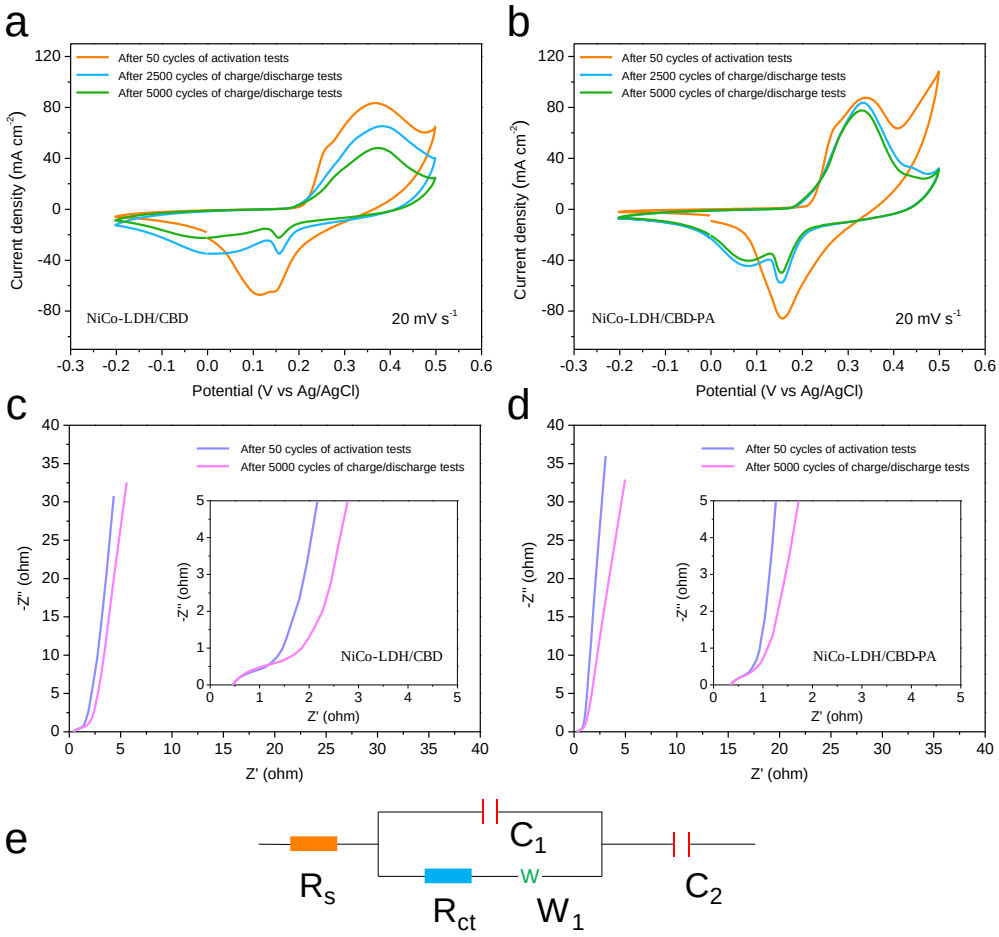

Sample	After 50 cycles of activation tests				After 5000 cycles of charge/discharge tests			
	R_s	R_{ct}	R_w	R_{ESR}	R_s	R_{ct}	R_w	R_{ESR}
NiCo-LDH/CBD	0.47	0.72	0.87	2.06	0.48	0.99	0.82	2.29
NiCo-LDH/CBD-PA	0.37	0.40	0.17	0.94	0.37	0.42	0.44	1.23

Fig. S14. The CV curves and EIS spectra of NiCo-LDH/CBD-PA and NiCo-LDH/CBD samples during cycling tests in 6 M KOH solution. (a, b) CV curves. (c, d) EIS spectra. (e) The equivalent circuit diagram and the detailed values of R_s, R_{ct}, R_w, and R_{ESR} for NiCo-LDH/CBD and NiCo-LDH/CBD-PA.

The definition of R_s, R_{ct}, R_w, and R_{ESR} are as follows [S1].

R_s (intrinsic Ohmic resistance) mainly comes from the intrinsic resistance of electrode material, electrolyte, current collector and leads, as well as the contact resistances between them.

R_{ct} (charge transfer resistance) mainly comes from the electronic and ionic resistances at the interface between the electrode and the electrolyte. This resistance mainly depends on the charge transport kinetics (*i.e.*, the matching degree between electrons and ions) during the redox reaction, the wettability between electrolyte and electrode, and the morphology and conductivity of electrode. In addition, the ion transfer distance and the temperature can also influence the value of R_{ct}.

R_w (Warburg diffusion resistance) comes from the resistance for ion diffusion from electrolyte into the electrodes. R_w also depends on the influencing factors for R_{ct}.

R_{ESR} (equivalent series resistance) contains R_s, R_{ct}, and R_w. The detailed values of the R_s, R_{ct}, and

R_w for NiCo-LDH/CBD and NiCo-LDH/CBD-PA sample are obtained by simulating the Nyquist plots with Z Fit-Bio-Logic method of the EC-Lab software (V11.01), and shown in Fig. S14e.

The CV curves were recorded after 50 cycles of activation tests (*i.e.*, before the cycling tests), and after 2500 and 5000 cycles of charge/discharge tests. With increasing the cycle number, the area of CV curves decreases gradually, indicating a gradual decay of the specific capacitance. Comparatively speaking, the area of CV curves for NiCo-LDH/CBD-PA decreases more slowly than the case for NiCo-LDH/CBD (Fig. S14a, b), which indicates the better cycling stability of NiCo-LDH/CBD-PA than NiCo-LDH/CBD.

After charge/discharge tests, the NiCo-LDH/CBD-PA presents smaller values of R_{ct} and R_w than the NiCo-LDH/CBD, leading to the smaller R_{ESR} and better charge transfer kinetics of the former (Fig. S14e).

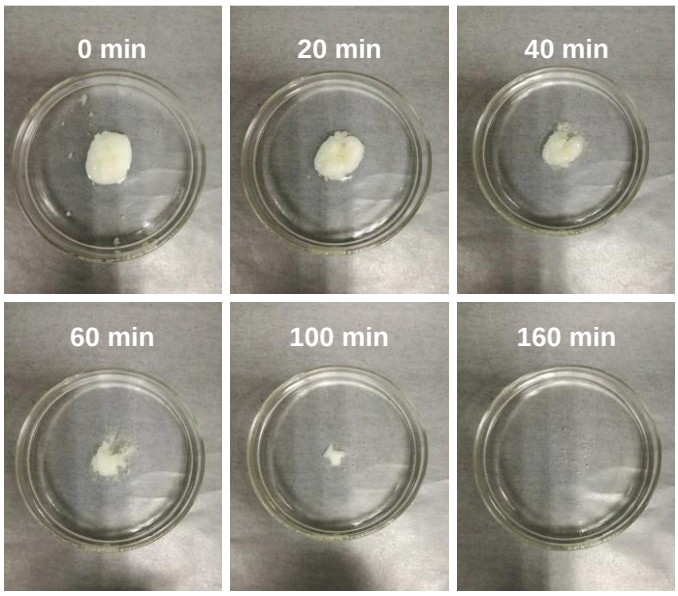

Fig. S15. The dissolution test of PA in 6 M KOH electrolyte.

It is indicated that the PA can be dissolved in 6 M KOH electrolyte.

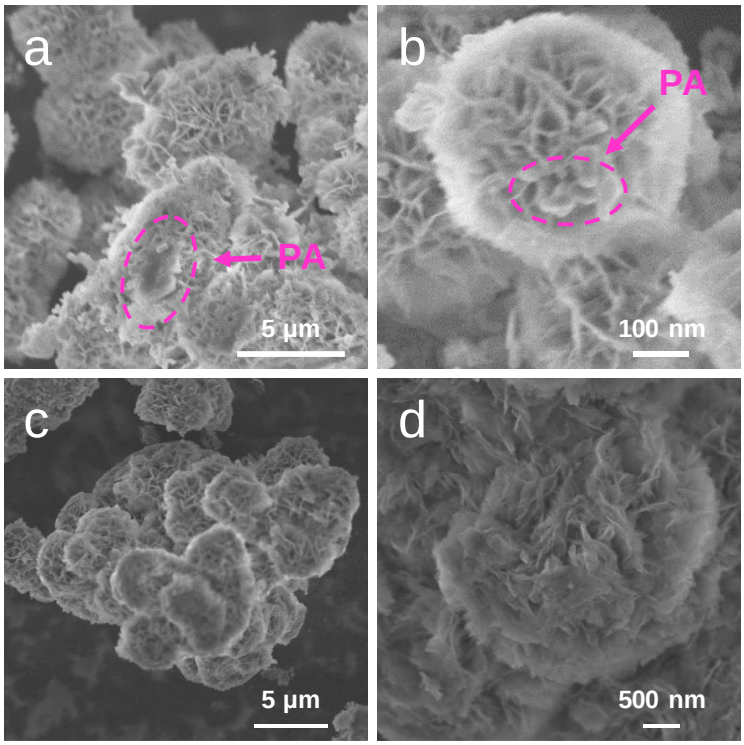

Fig. S16. Morphology of NiCo-LDH/CBD-PA before and after cycling test. (a, b) SEM images of pristine NiCo-LDH/CBD-PA. (c, d) SEM images of NiCo-LDH/CBD-PA after 5000 cycles.

PA particles can be observed on the pristine NiCo-LDH/CBD-PA sample (a, b). After 5000 cycles, the LDHs surface is quite clean (c, d), which indicates the dissolution of PA.

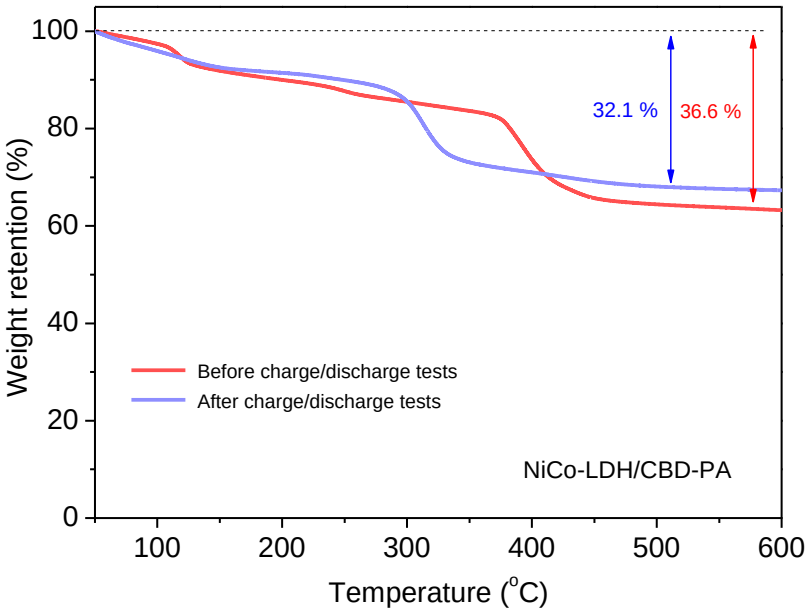

Fig. S17. TG analysis of NiCo-LDH/CBD-PA sample before and after 5000 cycles test [heating rate: 5 ℃ min^{-1}, N_2].

The total weight loss of NiCo-LDH/CBD-PA sample after long-term charge/discharge test (32.1%) is lower than that of the sample before cycling test (36.6%), which indicates that partial PA polymer was dissolved into electrolyte during the long-term charge/discharge tests.

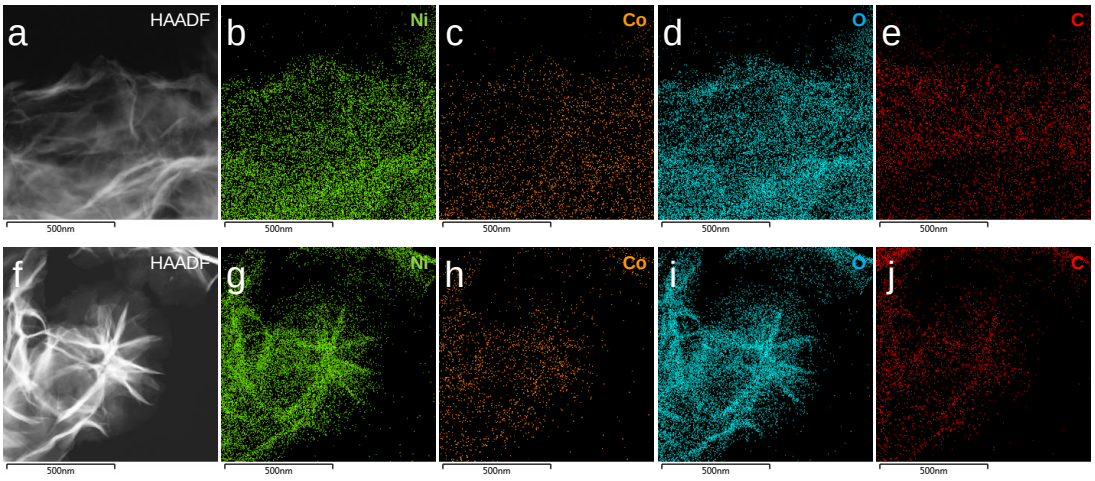

k

Sample	The atomic percentage before cycling tests (%)				The atomic percentage after cycling tests (%)			
	Ni	Co	O	C	Ni	Co	O	C
NiCo-LDH /CBD-PA	12.27	2.42	52.15	33.15	19.24	3.79	61.48	15.49

Fig. S18. HAADF image and the corresponding EDX element mappings of NiCo-LDH/CBD-PA. (a-e) Before cycling test. (f-j) After test for 5000 cycles. (k) The atomic percentage before/after cycling test.

To compare the PA content in the NiCo-LDH/CBD-PA before and after the electrochemical test for 5000 cycles, HAADF observation and the corresponding EDX element mappings were performed. Generally, the LDH samples show uniform element distributions for Ni, Co, O and C (Fig. S18a-j). The C element mainly comes from PA, which shows much lower content for the sample after cycling test than that before cycling (Fig. S18k). This result supports the loss of PA polymer during the cycling test.

References

[S1] J. Zhao, C. Ge, Z. Zhao, Q. Wu, M. Liu, M. Yan, L. Yang, X. Wang and Z. Hu, *Nano Energy*, 2020, **76**, 105026.

[S2] J. Xiong, H. Shen, J. Mao, X. Qin, P. Xiao, X. Wang, Q. Wu and Z. Hu, *J. Mater. Chem.*, 2012, **22**, 11927–11932.

[S3] H. Lai, Q. Wu, J. Zhao, L. Shang, H. Li, R. Che, Z. Lyu, J. Xiong, L. Yang, X. Wang and Z. Hu, *Energy Environ. Sci.*, 2016, **9**, 2053–2060.

[S4] P. Vialat, C. Mousty, C. Taviot-Gueho, G. Renaudin, H. Martinez, J.-C. Dupin, E. Elkaim and F. Leroux, *Adv. Funct. Mater.*, 2014, **24**, 4831–4842.

[S5] I. Shakir, M. Shahid, U.A. Rana, I.M.A. Nashef and R. Hussain, *Electrochim. Acta*, 2014, **129**, 28–32.

[S6] X. Ge, C.D. Gu, X.L. Wang and J.P. Tu, *J. Mater. Chem. A*, 2014, **2**, 17066–17076.

[S7] X. Li, J. Zai, Y. Liu, X. He, S. Xiang, Z. Ma and X. Qian, *J. Power Sources*, 2016, **325**, 675–681.

[S8] X. Wang, C. Yan, A. Sumboja, J. Yan and P.S. Lee, *Adv. Energy Mater.*, 2014, **4**, 1301240.

[S9] L. Wang, Z.H. Dong, Z.G. Wang, F.X. Zhang and J. Jin, *Adv. Funct. Mater.*, 2013, **23**, 2758–2764.

[S10] X. Wang, Y. Lin, Y. Su, B. Zhang, C. Li, H. Wang and L. Wang, *Electrochim. Acta*, 2017, **225**, 263–271.

[S11] J.P. Cheng, J.H. Fang, M. Li, W.F. Zhang, F. Liu and X.B. Zhang, *Electrochim. Acta*, 2013, **114**, 68–75.